Electronic Supplementary Material (ESI) for Physical Chemistry Chemical Physics.

Supplementary Information for: Evaluation of Mixed Quantum-Classical Molecular Dynamics on *cis*-Azobenzene Photoisomerization

Diandong Tang, Lin Shen* and Wei-Hai Fang

Key Laboratory of Theoretical and Computational Photochemistry of Ministry of Education, College of Chemistry, Beijing Normal University, Beijing 100875, China

E-mail: lshen@bnu.edu.cn

Collective Dynamics of PC-FBD & PC-EBD

Table S1: Simulation results using PC-FBD and PC-EBD in comparison with experimental results.

MQC Method	Decoherence	Rescaling	S_1 lifetime ± standard error (fs)	*trans*-isomer yield
FSSH	PC-EBD	$E+$	93.0 ± 0.4	0.522
		$E\mathbf{p_h}+$	65.0 ± 0.4	0.675
		$E\mathbf{p_h}-$	67.3 ± 0.4	0.570
	PC-FBD	$E+$	92.5 ± 0.3	0.486
		$E\mathbf{p_h}+$	66.1 ± 0.4	0.665
		$E\mathbf{p_h}-$	67.4 ± 0.4	0.575
expr.			100-170	0.40-0.75

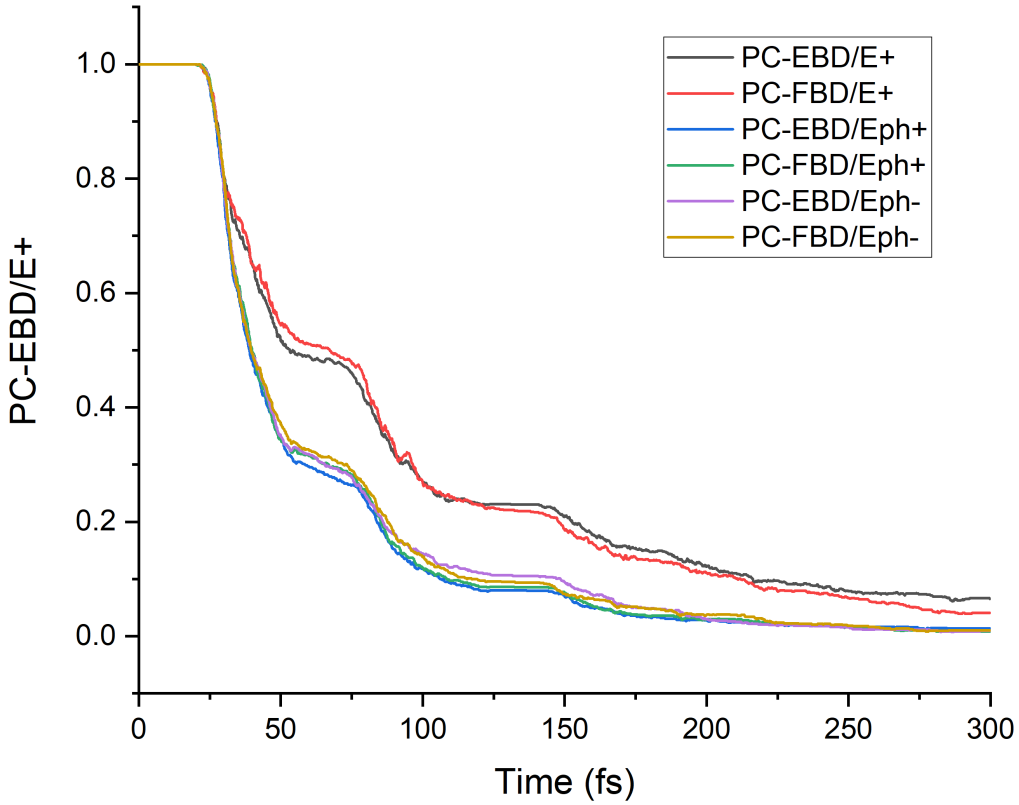

Figure S1: Time-dependent electronic state populations obtained using PC-EBD and PC-FBD.

Representative Trajectories for all Simulations

Table S2: List of Representative Trajectories

FSSH/E+	Figure 3(a)	EMF	Figure 5(a)
FSSH/$E\mathbf{p_h}$+	Figure S2	PC-EMF	Figure 5(b)
FSSH/$E\mathbf{p_h}$−	Figure S3	MFSD	Figure 5(c)
EBD/E+	Figure S4	PC-MFSD	Figure S20
EBD/$E\mathbf{p_h}$+	Figure S5	PC-BCMF	Figure 5(d)
EBD/$E\mathbf{p_h}$−	Figure S6	QTMF[a]	Figure 5(e)
FBD/E+	Figure 3(c)	QTMF[b]	Figure S21
FBD/$E\mathbf{p_h}$+	Figure 4(a)	MM/SQC[c]	Figure 6(a)
FBD/$E\mathbf{p_h}$−	Figure 4(b)	MM/SQC[d]	Figure 6(b)
PCSH/E+	Figure 3(b)		
PCSH/$E\mathbf{p_h}$+	Figure S7		
PCSH/$E\mathbf{p_h}$−	Figure S8		
BCSH/E+	Figure S9		
BCSH/$E\mathbf{p_h}$+	Figure S10		
BCSH/$E\mathbf{p_h}$−	Figure S11		
PC-BCSH/E+	Figure 3(d)		
PC-BCSH/$E\mathbf{p_h}$+	Figure S12		
PC-BCSH/$E\mathbf{p_h}$−	Figure S13		
PC-EBD/E+	Figure S14		
PC-EBD/$E\mathbf{p_h}$+	Figure S15		
PC-EBD/$E\mathbf{p_h}$−	Figure S16		
PC-FBD/E+	Figure S17		
PC-FBD/$E\mathbf{p_h}$+	Figure S18		
PC-FBD/$E\mathbf{p_h}$−	Figure S19		

(a) Decoherence rate was fixed as 0.001. (b) Decoherence rate was determined on-the-fly. (c) Linear window function with parameter as 0.500. (d) Square window function with parameter as 0.366.

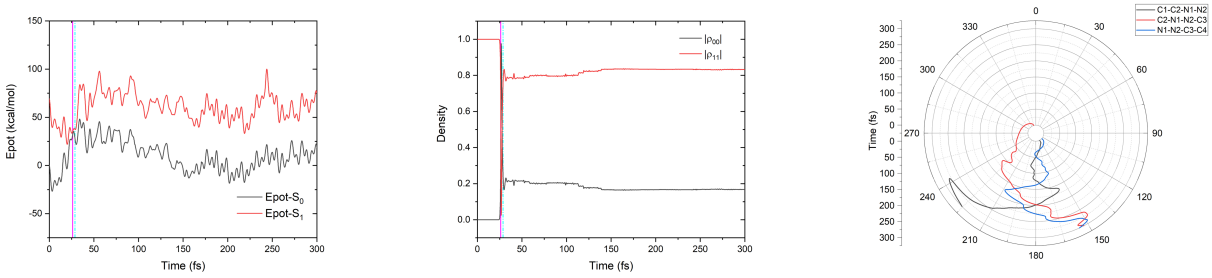

Figure S2: Time evolution of adiabatic potential energy (left), electronic populations (middle) and the dihedral angles C1-C2-N1-N2, C2-N1-N2-C3 and N1-N2-C3-C4 (right) for FSSH/$E\mathbf{p_h}+$.

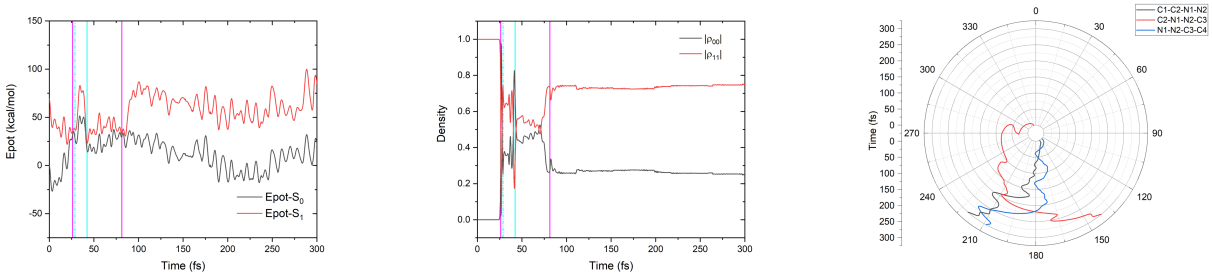

Figure S3: Time evolution of adiabatic potential energy (left), electronic populations (middle) and the dihedral angles C1-C2-N1-N2, C2-N1-N2-C3 and N1-N2-C3-C4 (right) for FSSH/$E\mathbf{p_h}-$.

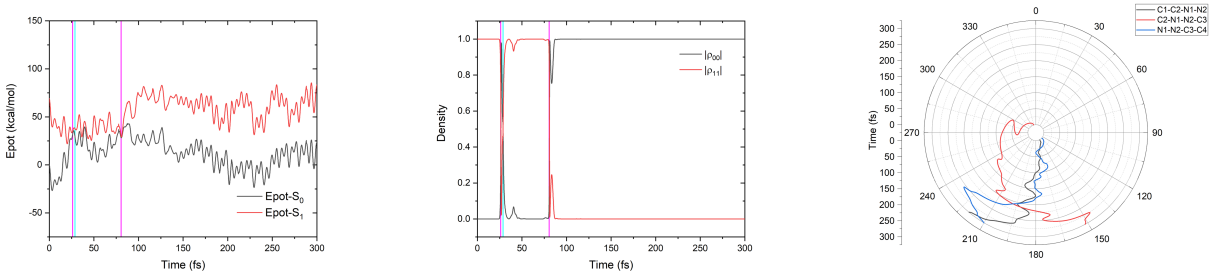

Figure S4: Time evolution of adiabatic potential energy (left), electronic populations (middle) and the dihedral angles C1-C2-N1-N2, C2-N1-N2-C3 and N1-N2-C3-C4 (right) for EBD/E+.

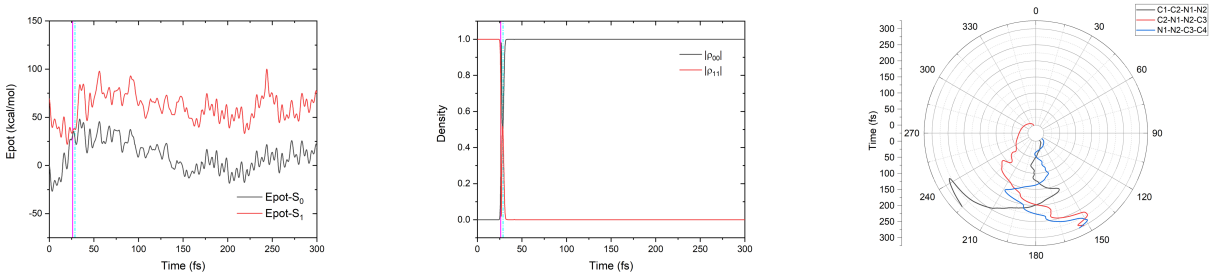

Figure S5: Time evolution of adiabatic potential energy (left), electronic populations (middle) and the dihedral angles C1-C2-N1-N2, C2-N1-N2-C3 and N1-N2-C3-C4 (right) for EBD/$E\mathbf{p_h}$+.

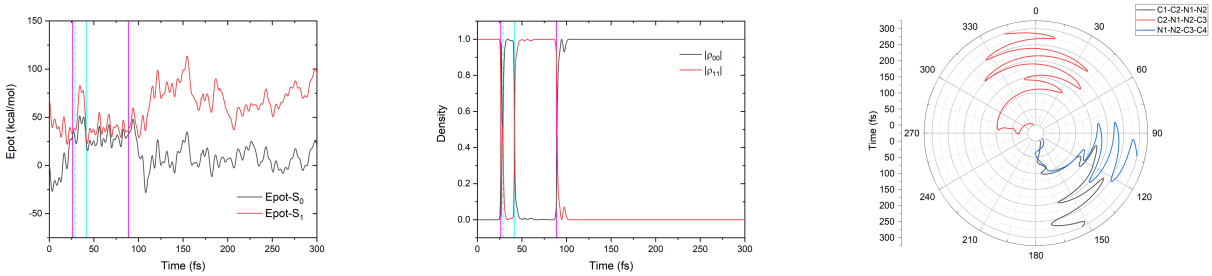

Figure S6: Time evolution of adiabatic potential energy (left), electronic populations (middle) and the dihedral angles C1-C2-N1-N2, C2-N1-N2-C3 and N1-N2-C3-C4 (right) for EBD/$E\mathbf{p_h}-$.

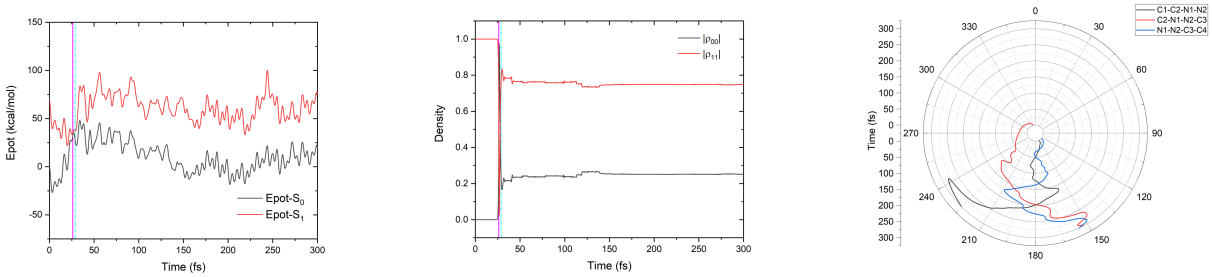

Figure S7: Time evolution of adiabatic potential energy (left), electronic populations (middle) and the dihedral angles C1-C2-N1-N2, C2-N1-N2-C3 and N1-N2-C3-C4 (right) for PCSH/$E\mathbf{p_h}$+.

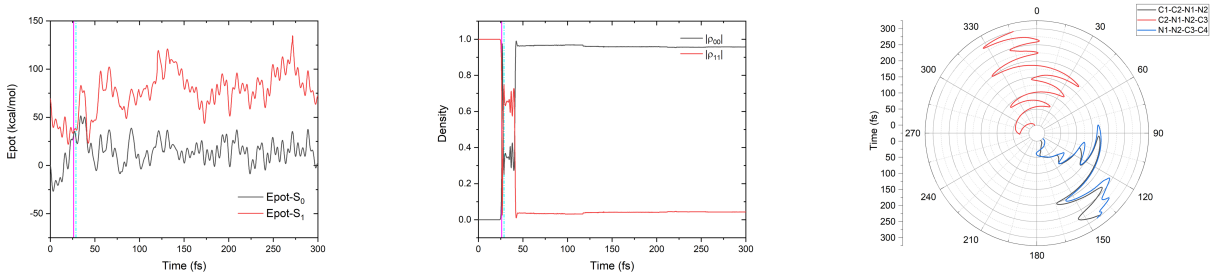

Figure S8: Time evolution of adiabatic potential energy (left), electronic populations (middle) and the dihedral angles C1-C2-N1-N2, C2-N1-N2-C3 and N1-N2-C3-C4 (right) for PCSH/$E\mathbf{p_h}-$.

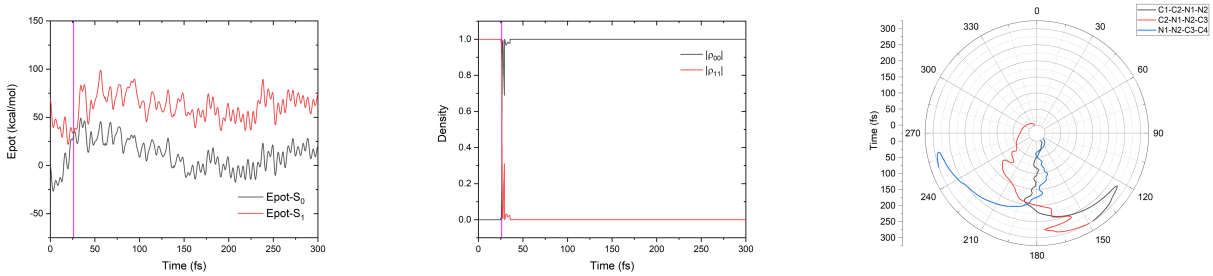

Figure S9: Time evolution of adiabatic potential energy (left), electronic populations (middle) and the dihedral angles C1-C2-N1-N2, C2-N1-N2-C3 and N1-N2-C3-C4 (right) for BCSH/E+.

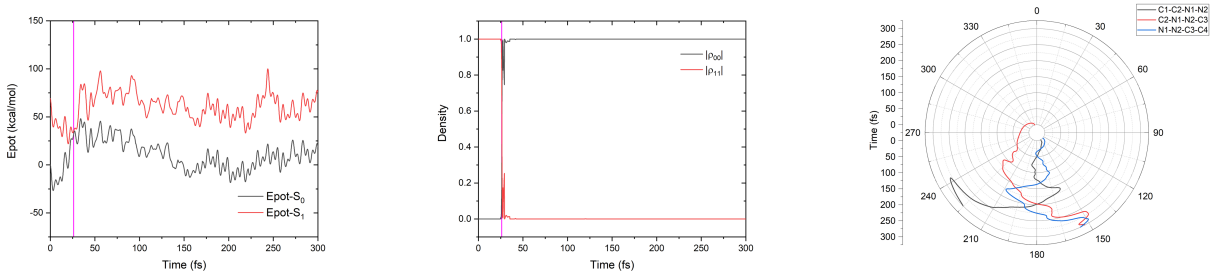

Figure S10: Time evolution of adiabatic potential energy (left), electronic populations (middle) and the dihedral angles C1-C2-N1-N2, C2-N1-N2-C3 and N1-N2-C3-C4 (right) for BCSH/$E\mathbf{p_h}+$.

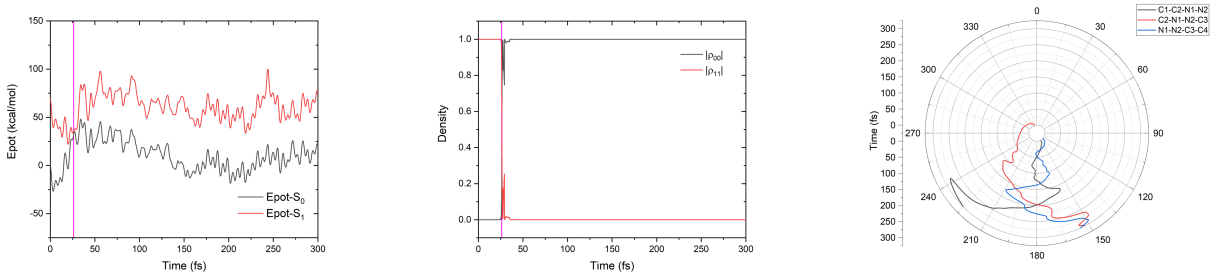

Figure S11: Time evolution of adiabatic potential energy (left), electronic populations (middle) and the dihedral angles C1-C2-N1-N2, C2-N1-N2-C3 and N1-N2-C3-C4 (right) for BCSH/$E\mathbf{p_h}-$.

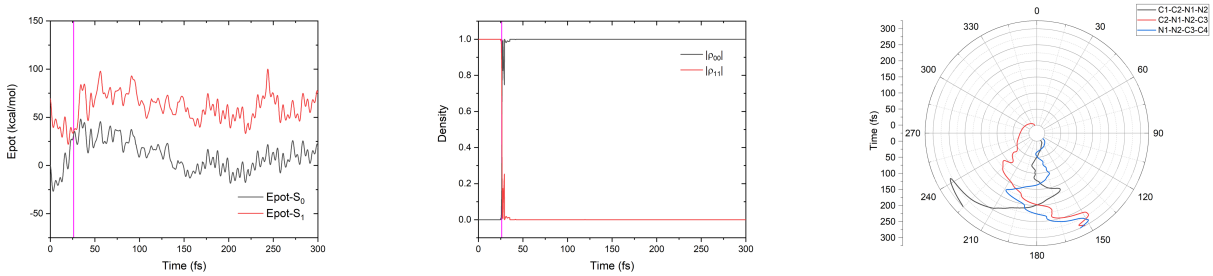

Figure S12: Time evolution of adiabatic potential energy (left), electronic populations (middle) and the dihedral angles C1-C2-N1-N2, C2-N1-N2-C3 and N1-N2-C3-C4 (right) for PC-BCSH/$E\mathbf{p_h}+$.

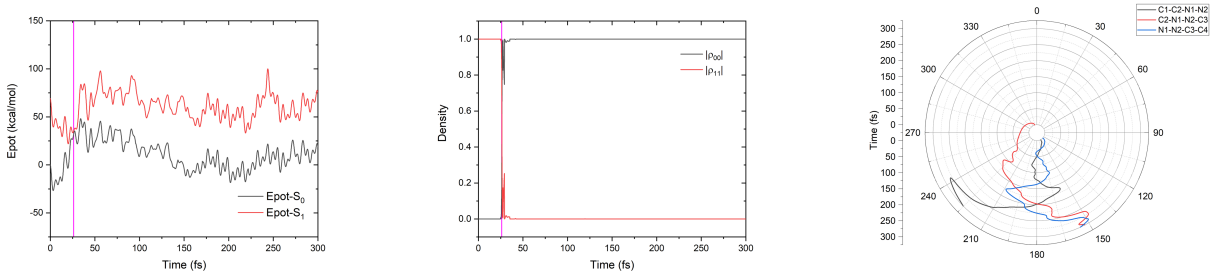

Figure S13: Time evolution of adiabatic potential energy (left), electronic populations (middle) and the dihedral angles C1-C2-N1-N2, C2-N1-N2-C3 and N1-N2-C3-C4 (right) for PC-BCSH/$E\mathbf{p_h}-$.

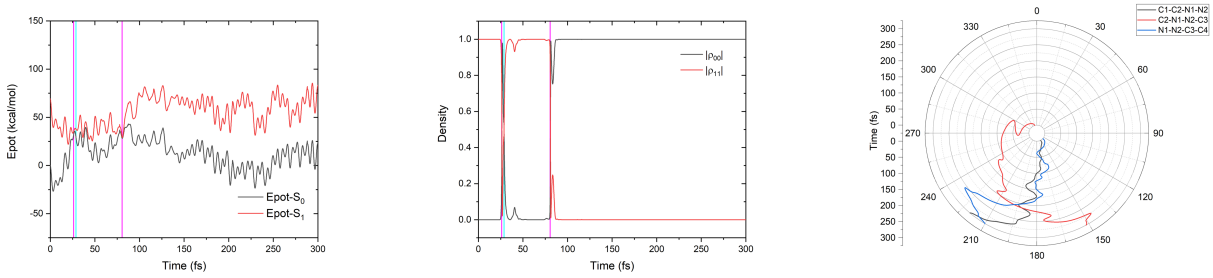

Figure S14: Time evolution of adiabatic potential energy (left), electronic populations (middle) and the dihedral angles C1-C2-N1-N2, C2-N1-N2-C3 and N1-N2-C3-C4 (right) for PCEBD/E+.

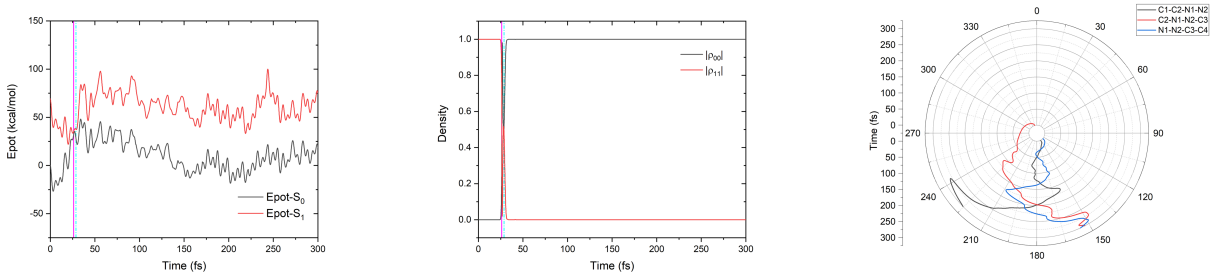

Figure S15: Time evolution of adiabatic potential energy (left), electronic populations (middle) and the dihedral angles C1-C2-N1-N2, C2-N1-N2-C3 and N1-N2-C3-C4 (right) for PCEBD/$E_{\mathbf{p_h}}$+.

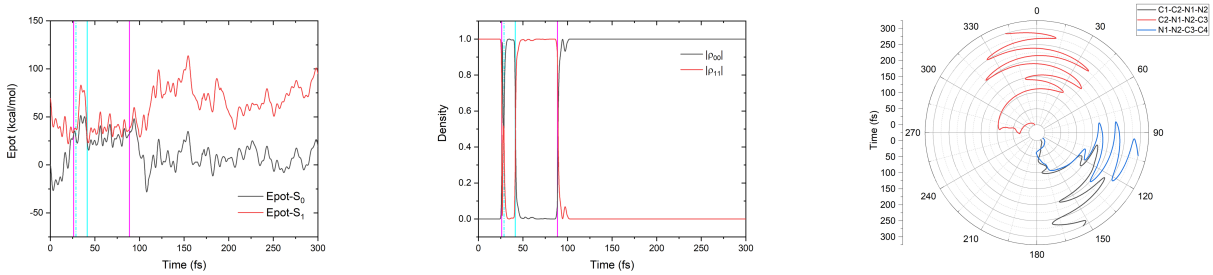

Figure S16: Time evolution of adiabatic potential energy (left), electronic populations (middle) and the dihedral angles C1-C2-N1-N2, C2-N1-N2-C3 and N1-N2-C3-C4 (right) for PCEBD/$E_{\mathbf{p_h}}$−.

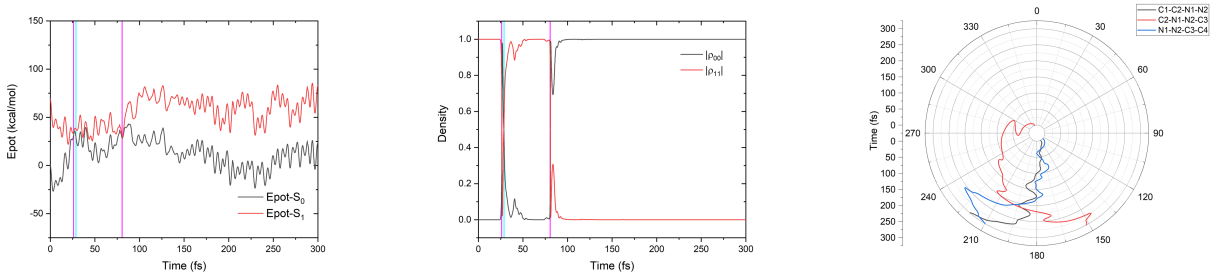

Figure S17: Time evolution of adiabatic potential energy (left), electronic populations (middle) and the dihedral angles C1-C2-N1-N2, C2-N1-N2-C3 and N1-N2-C3-C4 (right) for PC-FBD/E+.

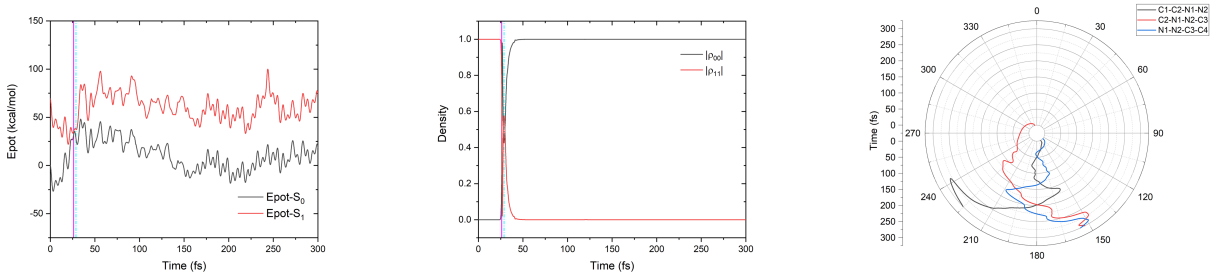

Figure S18: Time evolution of adiabatic potential energy (left), electronic populations (middle) and the dihedral angles C1-C2-N1-N2, C2-N1-N2-C3 and N1-N2-C3-C4 (right) for PC-FBD/$E\mathbf{p_h}$+.

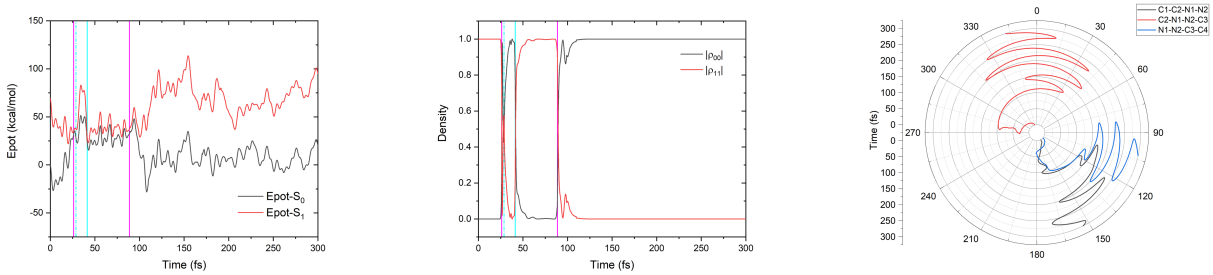

Figure S19: Time evolution of adiabatic potential energy (left), electronic populations (middle) and the dihedral angles C1-C2-N1-N2, C2-N1-N2-C3 and N1-N2-C3-C4 (right) for PC-FBD/$E\mathbf{p_h}$−.

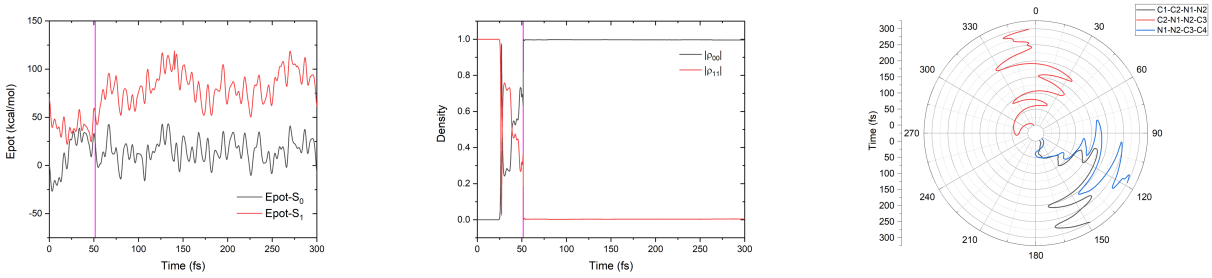

Figure S20: Time evolution of adiabatic potential energy (left), electronic populations (middle) and the dihedral angles C1-C2-N1-N2, C2-N1-N2-C3 and N1-N2-C3-C4 (right) for PC-MFSD.

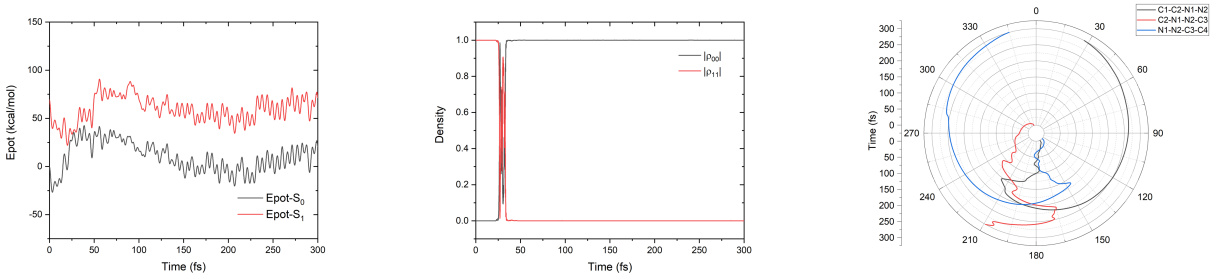

Figure S21: Time evolution of adiabatic potential energy (left), electronic populations (middle) and the dihedral angles C1-C2-N1-N2, C2-N1-N2-C3 and N1-N2-C3-C4 (right) for QTMF in which the decoherence rate was determined on-the-fly.

Effects of Momentum Rescaling

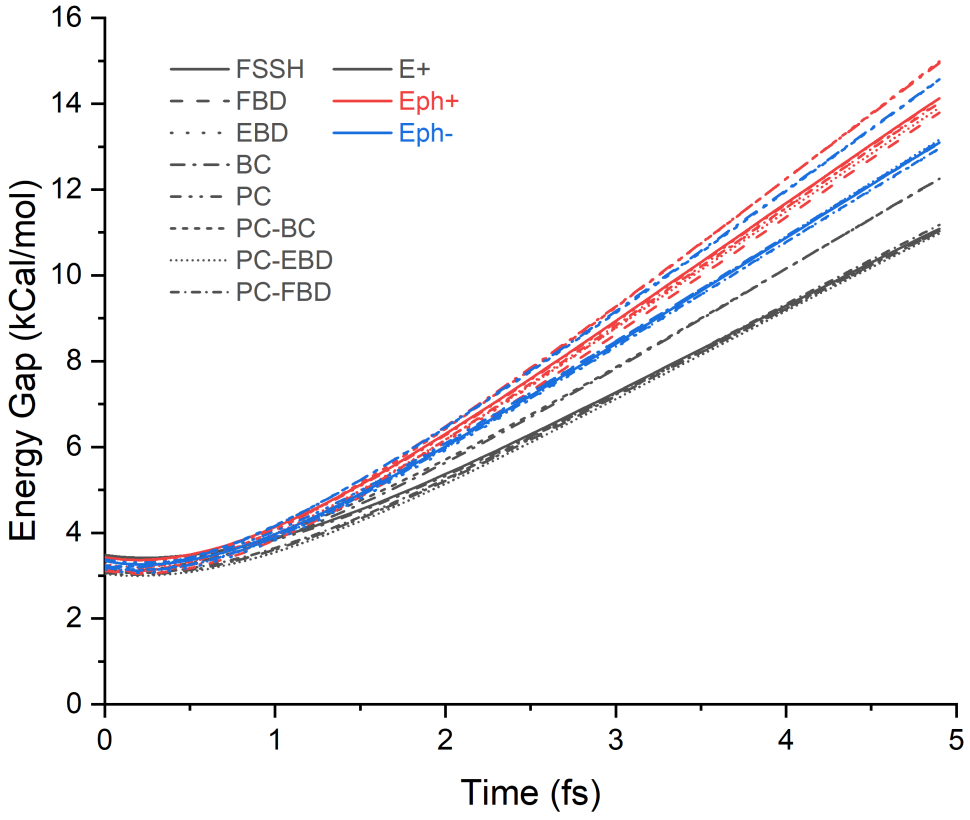

Figure S22: Energy gap between S_1 and S_0 plotted as a function of time after hopping event from S_1 to S_0 averaged on all trajectories using different models.

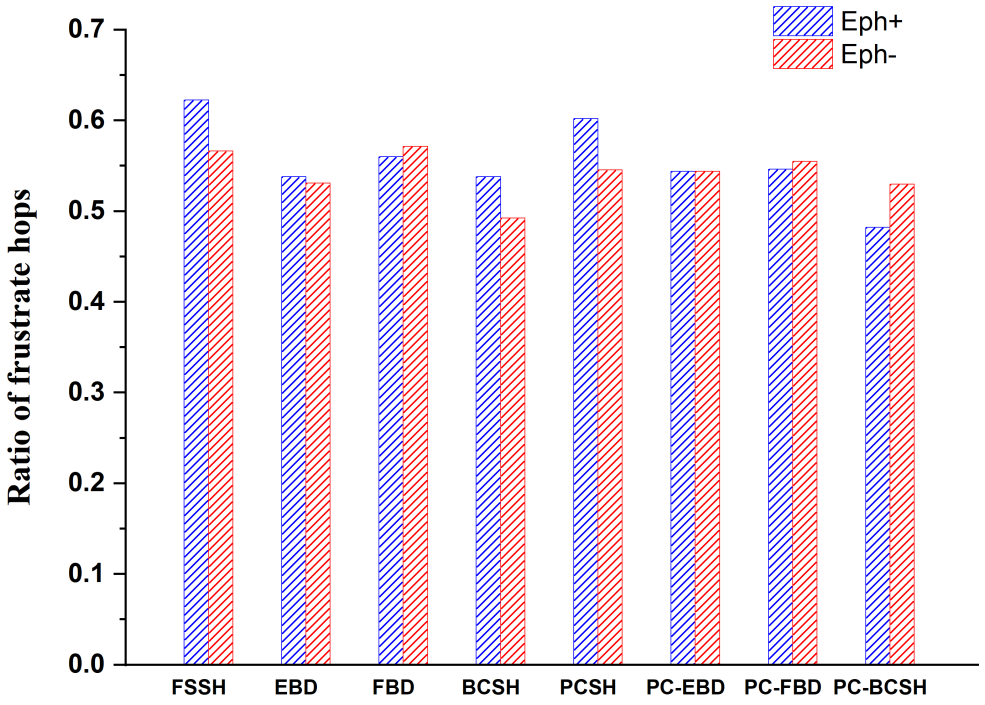

Figure S23: Ratio of frustrated hops in all hopping-back attempts using different decoherence corrections with $E\mathbf{p_h}+$ and $E\mathbf{p_h}-$.

Distribution of Essential Geometry Parameters of Snapshots at which the Hop Occurs

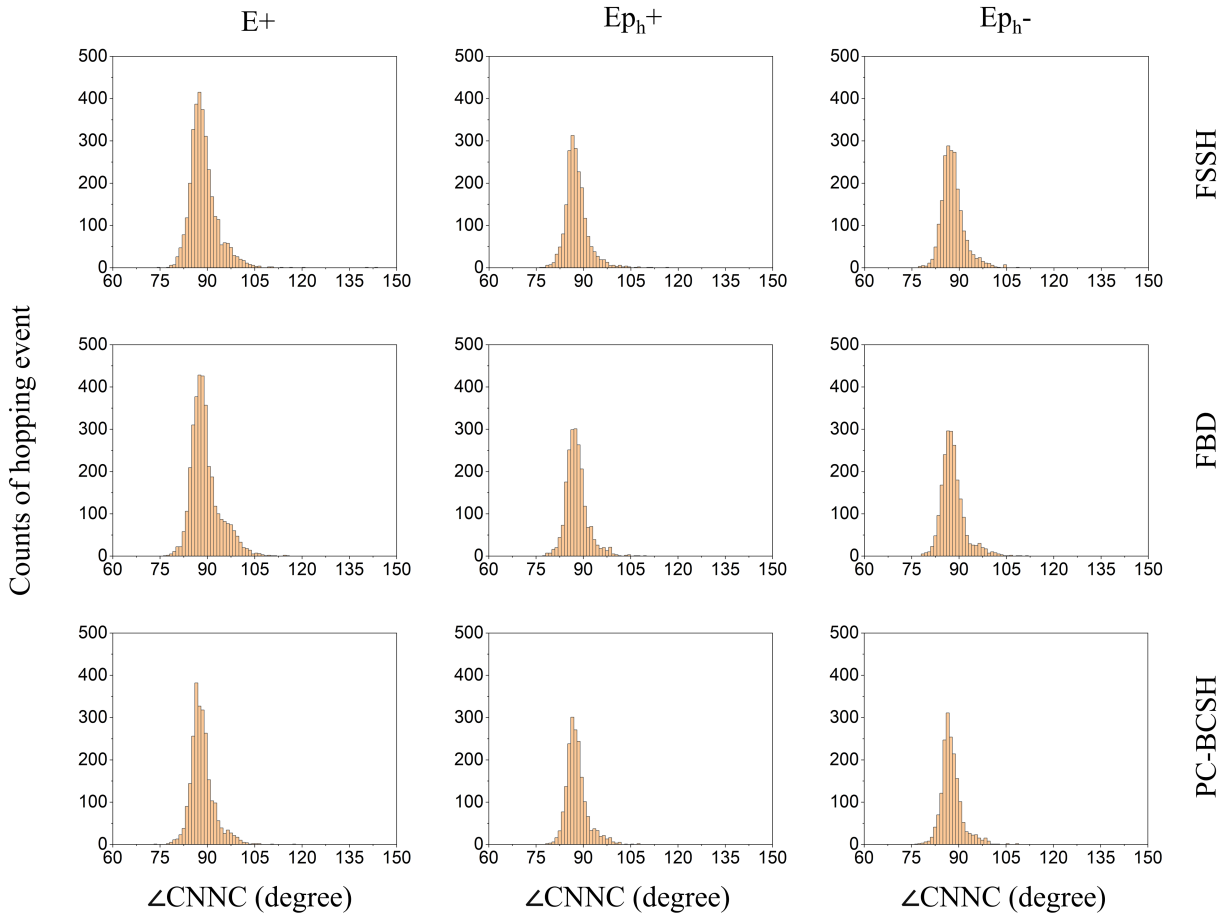

Figure S24: Distribution of C-N-N-C dihedral angle for all hopping events obtained using FSSH (top), FBD (middle) and PC-BCSH (bottom).

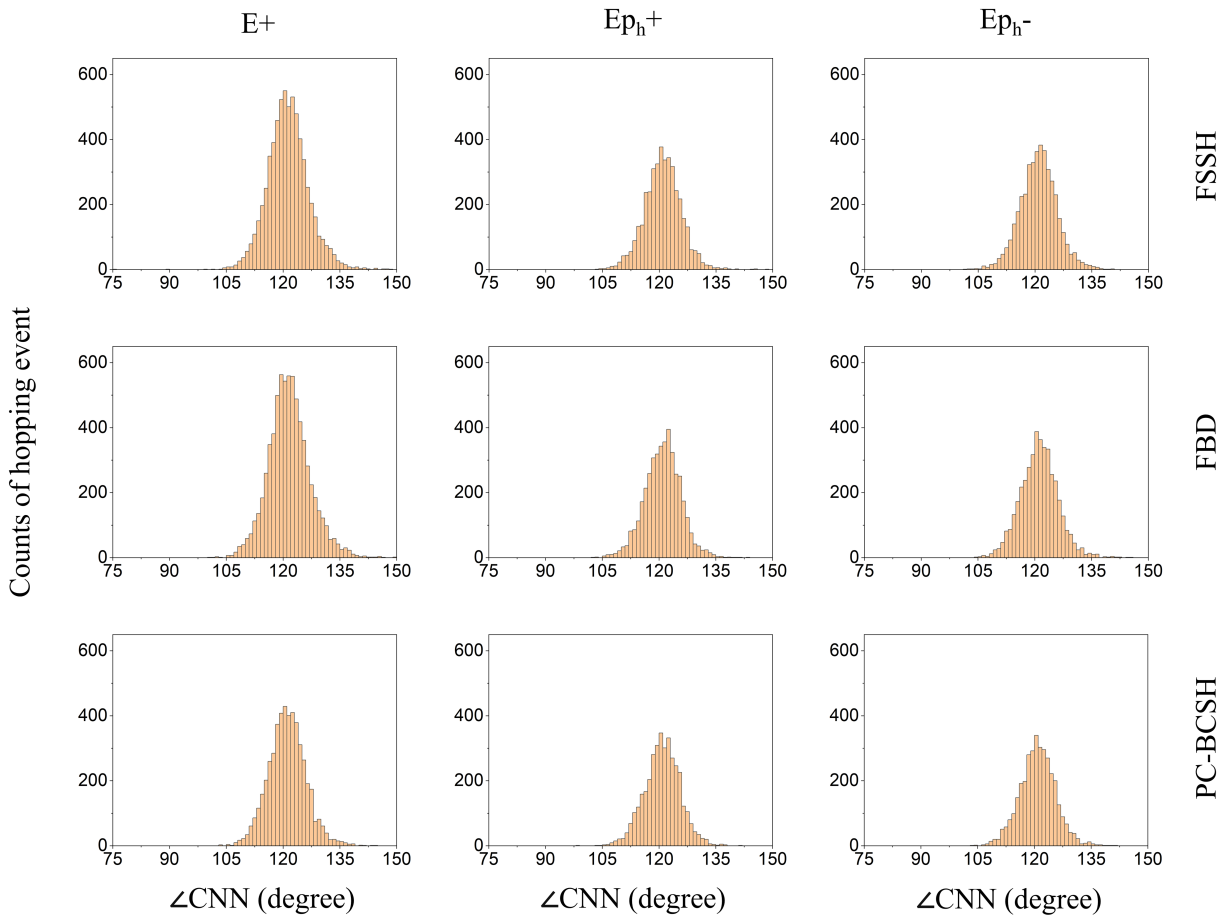

Figure S25: Distribution of C-N-N bending angles for all hopping events obtained using FSSH (top), FBD (middle) and PC-BCSH (bottom).

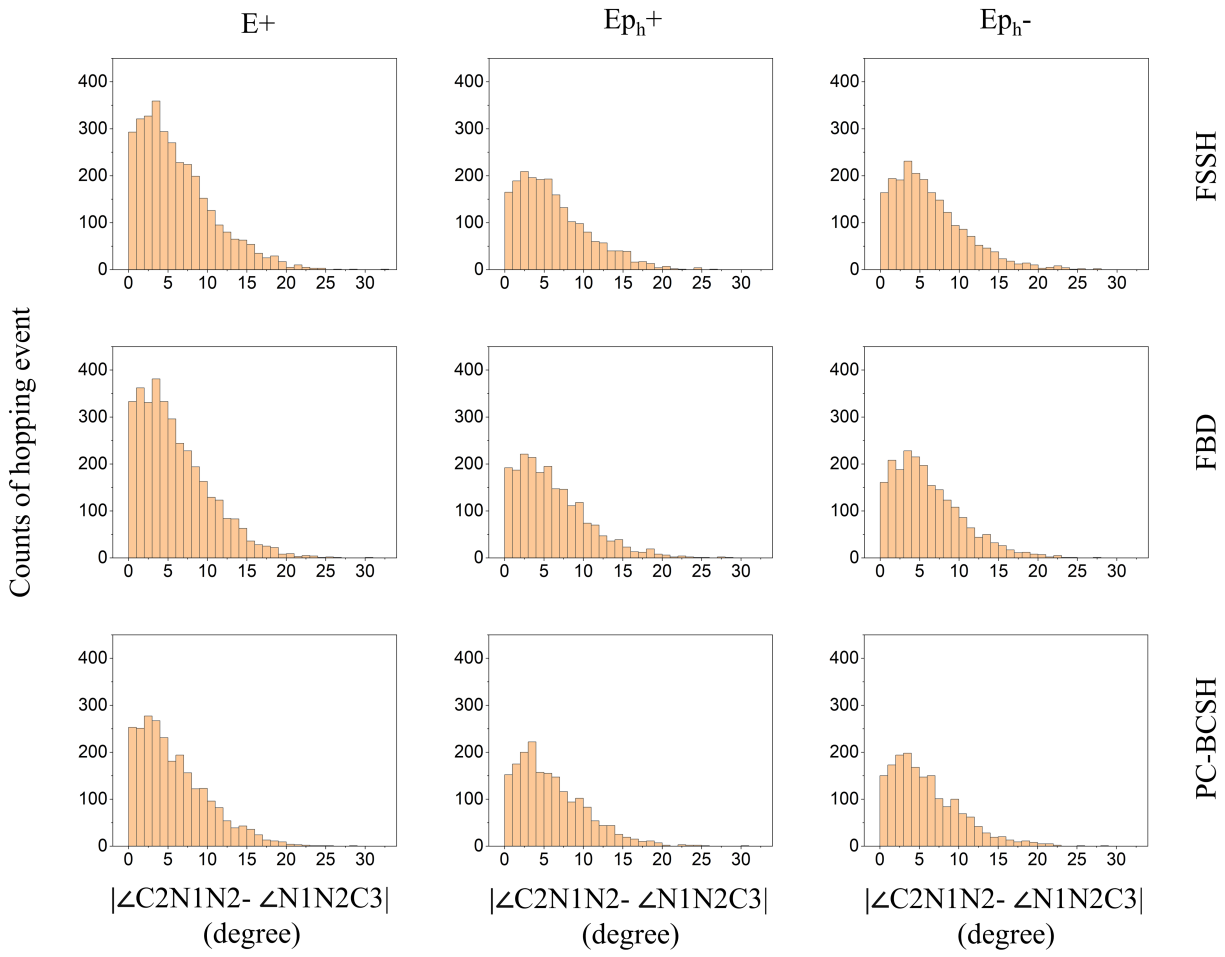

Figure S26: Distribution of the difference between two C-N-N bending angles for all hopping events obtained using FSSH (top), FBD (middle) and PC-BCSH (bottom).

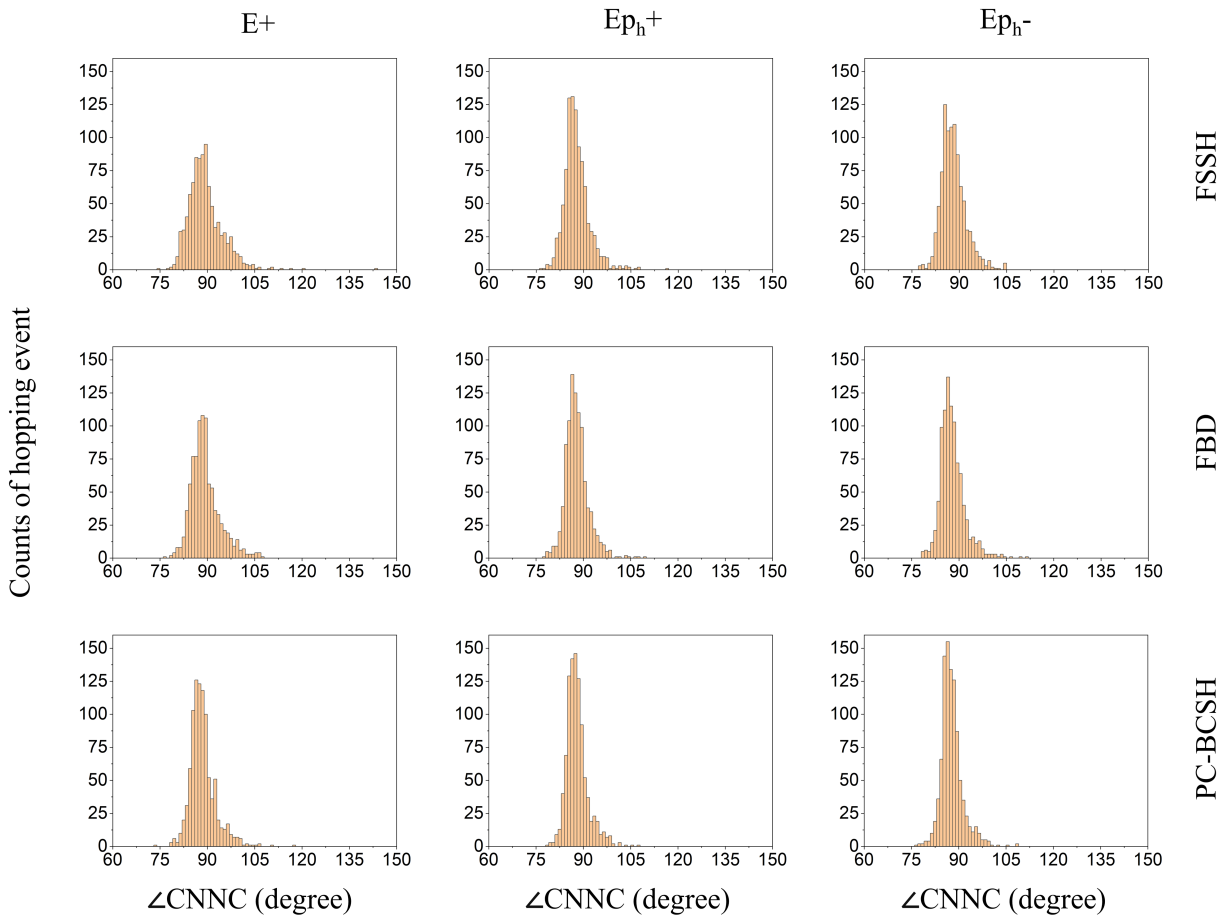

Figure S27: Distribution of C-N-N-C dihedral angle for the last $S_1 \rightarrow S_0$ hopping event for each trajectory using FSSH (top), FBD (middle) and PC-BCSH (bottom).

Data Availability

Source code and research data used in this study are available upon reasonable request to the corresponding author.